

# Solvent Engineering of Thermo-Responsive Hydrogels Facilitates Strong and Large Contractile Actuations

Yong Eun Cho, Jae-Man Park, Won Jun Song, Min-Gyu Lee, and Jeong-Yun Sun\*

Thermo-responsive hydrogels can generate the actuation force through volumetric transitions in response to temperature changes. However, their weak mechanical properties and fragile actuation performance limit robust applications. Existing approaches to enhance these properties have typically depended on additional components, leading to an unavoidable interference to the actuation performance. In this work, robust thermo-responsive hydrogels are fabricated through solvent engineering. A particular solvent, *N*-methylformamide, interacts affinitively with the carbonyl group of *N*-isopropylacrylamide monomer, solubilizes the monomer with extremely high concentration, stabilizes chain propagation during polymerization, and greatly increases chain lengths and entanglements of the resulting polymer. The synthesized hydrogels are highly elastic, strong, and tough, displaying remarkable thermo-responsive contractile actuation. The simple synthetic process can broaden its applicability in designing robust functional hydrogel applications.

## 1. Introduction

Poly(*N*-isopropylacrylamide) (pNIPAAm) is a distinctive type of stimuli-responsive polymer featured by its unique chemical structure. The polymer dissolves in water due to its hydrophilic amide groups, but above the lower critical solution temperature (LCST), the interaction between hydrophobic isopropyl and polymer backbone cause phase separation by collapsing interactions with water.<sup>[1]</sup> Therefore, when the pNIPAAm hydrogel network is heated to above the LCST, the water molecules are released from the gel, resulting in volumetric shrinkage that generates a contractile force. With a moderate LCST  $\approx 32^\circ\text{C}$  and the ability to undergo large volumetric changes (up to 90%) with biocompatibility, pNIPAAm hydrogels have been harnessed to apply them to diverse stimuli-responsive engineering fields, such

as soft actuators,<sup>[2]</sup> programming<sup>[3]</sup> or printing structures,<sup>[4]</sup> energy harvesting,<sup>[5]</sup> drug delivery<sup>[6]</sup> medical uses,<sup>[7]</sup> or neuromorphic device<sup>[8]</sup>

Nevertheless, their promising applicability has often been limited by their weak mechanical properties and frail actuation performances. Regular pNIPAAm hydrogels possess a strength of  $\approx 10\text{ kPa}$  and a fracture toughness of  $\approx 10\text{ J m}^{-2}$ , which makes them difficult to even handle.<sup>[1]</sup> Furthermore, the contraction force and energy density of pNIPAAm hydrogel are respectively  $\approx 3\text{ kPa}$  and  $\approx 10^{-2}\text{ kJ m}^{-3}$ , which is too weak to be used for engineering purposes. The improvement of mechanical properties of the pNIPAAm hydrogels has been achieved through the introduction of existing toughening or strengthening mechanism for hydrogels, such as interpenetrating network,<sup>[2a,i,9]</sup> incorporating

nanocomposite graphene oxide<sup>[2b]</sup> or nano clay<sup>[2a,10]</sup> or salt-induced crystallization.<sup>[11]</sup> However, these approaches for the mechanical enhancement of pNIPAAm hydrogels have compromised a certain actuation performance. The presence of non-responsive components inevitably reduces the proportion of responsive polymer networks, which in turn dilutes the transition qualitatively or quantitatively, resulting in low actuation strain or strength, or slow actuation speed. To achieve a complementary enhancement in both mechanical and actuation properties, therefore, an intrinsic mechanical enhancement of pNIPAAm hydrogels, without relying on additional components, is needed.

The weakness of pNIPAAm hydrogels originated from the low monomer solubility in water and the consequent short chain length between cross-links (**Figure 1B**). Traditionally, synthetic methods for robust pNIPAAm hydrogels often relied on the addition of external components rather than increasing the content of pNIPAAm itself. In this work, we aimed to unravel this limitation by elucidating the solvent effect on polymerization (**Figure 1**). We observed that when the polymerization solvent was replaced to ones with high monomer solubility, only a particular solvent, *N*-methylformamide (NMF), can facilitate the formation of highly long polymer chains and entangled networks. As a result, the mechanical behavior of the resulting pNIPAAm-only hydrogels was markedly distinguished by their mother solvents. The solvent effect on chain morphology and mechanical properties of the hydrogels was investigated. The wide solubility of NMF facilitates the engineering versatility of pNIPAAm hydrogels with enhanced actuation performance; 1) a small

Y. E. Cho, J.-M. Park, W. J. Song, M.-G. Lee, J.-Y. Sun  
Department of Materials Science and Engineering  
Seoul National University  
Seoul 08826, Republic of Korea  
E-mail: [jysun@snu.ac.kr](mailto:jysun@snu.ac.kr)

J.-Y. Sun  
Research Institute of Advanced Materials (RIAM)  
Seoul National University  
Seoul 08826, Republic of Korea

The ORCID identification number(s) for the author(s) of this article can be found under <https://doi.org/10.1002/adma.202406103>

DOI: 10.1002/adma.202406103

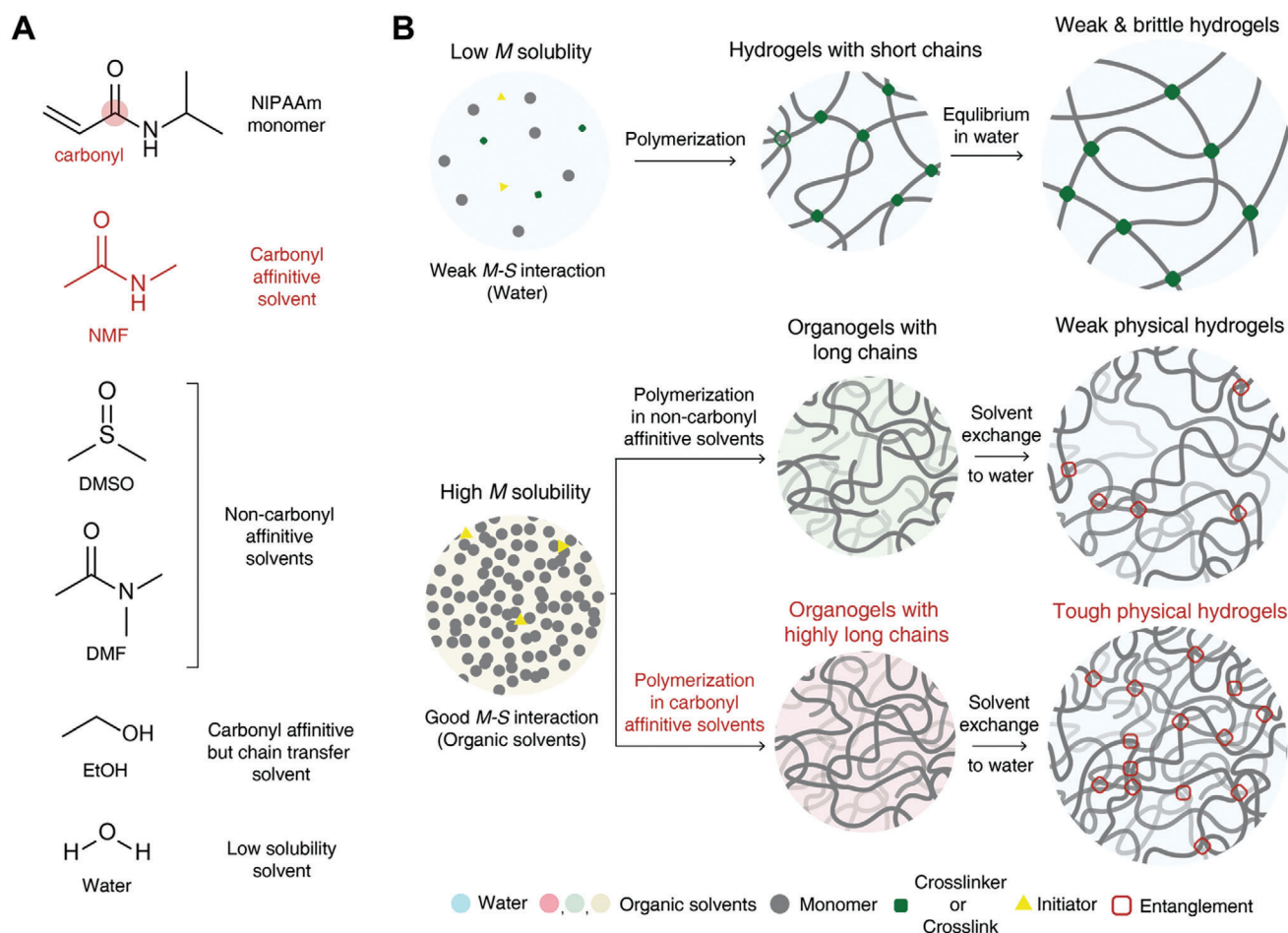


**Figure 1.** Synthetic strategies for making strong and tough poly(*N*-isopropylacrylamide) (pNIPAAm) hydrogels. A) Chemical structure of the NIPAAm monomer and various solvents used for polymerization. *N*-Methylformamide (NMF) is a carbonyl affinitive solvent for the NIPAAm monomer, while representative solvents for NIPAAm, such as dimethyl sulfoxide (DMSO) or *N,N*-dimethylformamide (DMF), are non-carbonyl affinitive solvents. Ethanol (EtOH) is a carbonyl-affinitive but chain transfer solvent. B) Schematic overview of the solvent engineering for the pNIPAAm hydrogel synthesis. Conventionally, the low solubility of NIPAAm monomers results in weak and brittle hydrogels due to relatively short chains. Alternatively, when the NIPAAm monomers are dissolved in highly soluble organic solvents and polymerized with a high monomer concentration, the resultant polymer could have long chains. In this case, the affinity between the monomer and the solvent significantly affects the chain length. Polymerization in a carbonyl affinitive solvent results in highly long polymer chains that induces more physical entanglements, culminating in the formation of physically robust hydrogels after a solvent exchange.

addition of co-monomers enables a facile modulation of LCST, 2) a small addition of water-insoluble cross-linkers enables an additional enhancement of mechanical and actuation performances, and 3) a small addition of inorganic gold nanoparticles enables robust light-driven actuation.

## 2. Results and Discussion

### 2.1. Solvent Engineering for Designing Strong and Tough pNIPAAm Hydrogels

To be a robust pNIPAAm hydrogel by itself, we thought that the chain lengths of the polymer should be sufficiently long, which can be realized by increasing the monomer concentration while decreasing the initiator concentration (Figure 1B). Thus, we screened various organic solvents that have high solubility of NIPAAm (Figure 2A). Four solvents, including NMF, dimethyl

sulfoxide (DMSO), *N,N*-dimethyl formamide (DMF), and ethyl alcohol (EtOH), were selected due to their high molal concentrations. We dissolved 2.4 g of the monomer in 1 g of those solvents, where the monomer concentration  $C_m$  is 21 m, added a small amount of the photoinitiator ( $10^{-5}$  mol.% compared to the monomer), and polymerized by ultraviolet light (see Experimental Section). The high concentration of monomer allowed for the formation of self-standing stiff organogel networks, and when the solvents were exchanged to equilibrate in water, the pNIPAAm hydrogels can be obtained with negligible residual organic solvent (Figure S1, Supporting Information). Hereafter, we refer to the pNIPAAm hydrogels synthesized by the above process in different solvents as Gel<sub>solvent</sub>. The fixed monomer concentration can exclude its effects on the degree of polymerization. The monomers in all solutions were mostly converted upon polymerization in all solvents (Figure S2, Supporting Information). Interestingly, the resulting Gel<sub>solvent</sub> exhibited distinct mechanical

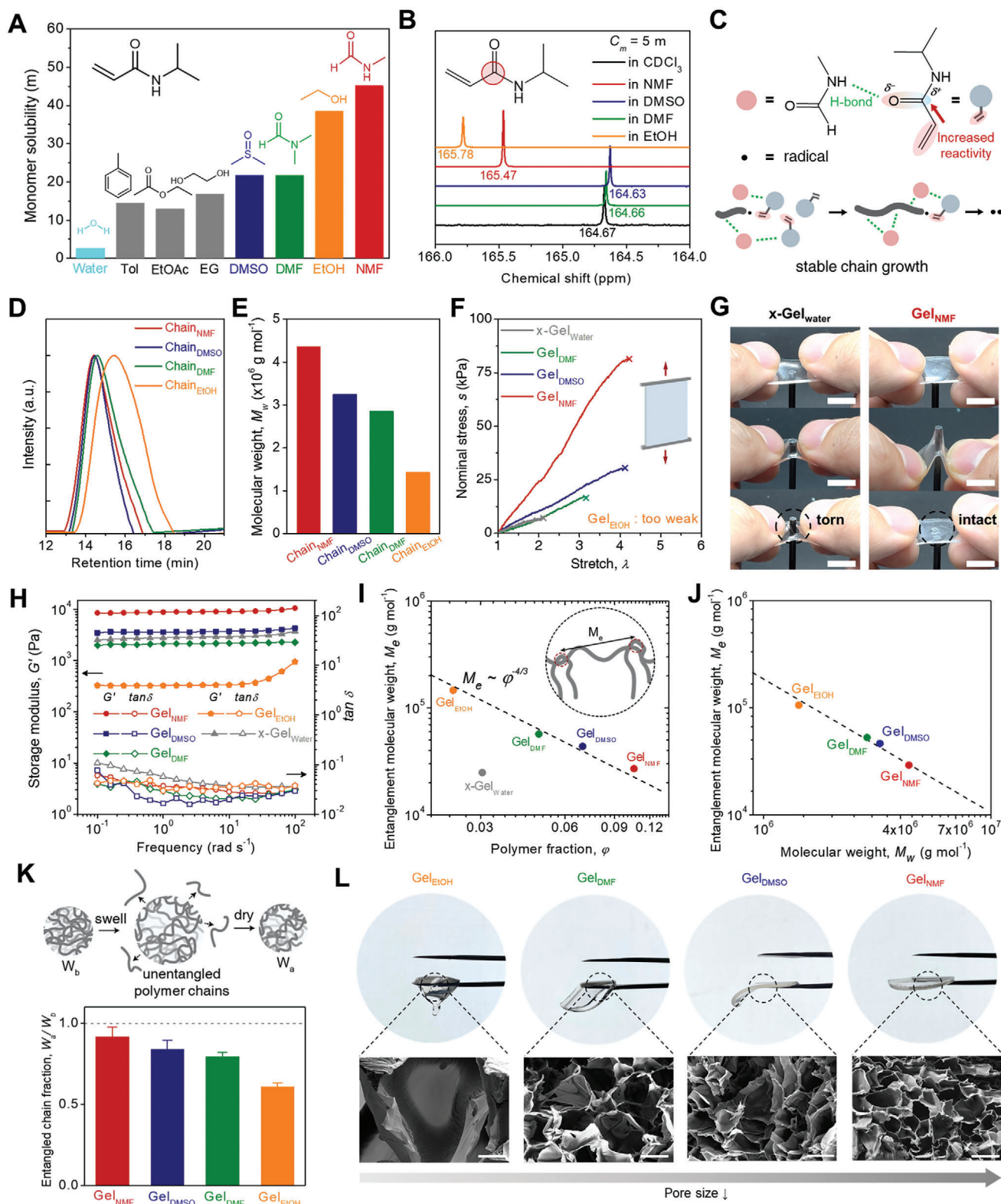


**Figure 2.** Solvent effect on mechanical properties and chain morphology of the pNIPAAm hydrogels. A) Solubility of the NIPAAm monomer in diverse solvents with their molecular structures. B) Chemical shifts for carbonyl ( $C=O$ ) C nuclei of the NIPAAm monomer in various organic solvents, where the monomer concentration  $C_m$  is 5 m. C) Schematic illustration of the carbonyl-affinitive solvent interacting with the NIPAAm monomer for stable polymer chain growth. D,E) Gel permeation chromatography (GPC) curves (D) and weight-average molecular weights  $M_w$  (E) of the solvent-engineered pNIPAAm chains. Polymers with  $C_m$  of 21 m is used for the measurement. F) Uniaxial stress-stretch curves of the Gel<sub>solvent</sub> with  $C_m$  of 21 m and the



properties, where the Gel<sub>NMF</sub> is taut while the Gel<sub>EtOH</sub> is flaccid (Figure S3 and Movie S1 Supporting Information).

The important point on the above synthetic process is that the type of solvents in polymerization greatly affects the mechanical properties of hydrogels. Since the interaction between the monomer and the solvent would influence the polymerization process, we examined the chemical shifts in nuclear magnetic resonance (NMR) spectroscopic analysis (Figure 2B; Figure S4, Supporting Information). In the same concentration of  $C_m = 5$  m, the chemical shifts of the C elements in the NIPAAm monomer were different by the type of solvents. Specifically, the carbonyl (C=O) C nucleus in the monomer exhibited an apparent red shift in EtOH and NMF, which indicates the affinitive hydrogen bonding of those solvents with the carbonyl nuclei of the monomer (Figure 2B). The affinitive hydrogen bonding of NMF with the monomer was further confirmed with Fourier transform infrared (FT-IR) spectroscopy, where the carbonyl (C=O) stretching vibrational band of the monomer shifts to lower wavenumber due to intermolecular hydrogen bonding with NMF (Figure S5, Supporting Information). While DMF and DMSO were non-affinitive with the carbonyl nucleus, which rather induces the shift in the isopropyl C nuclei, meaning that those solvents are affinitive with the isopropyl nuclei (Figure S4, Supporting Information). These different interaction site of the solvents with the monomer can be attributed to their molecular structures, where the protic solvents (NMF and EtOH) are able to interact with the amide group of the monomer by the affinitive hydrogen bonding, whereas the aprotic solvents (DMSO and DMF) are not. The affinitive hydrogen bonding of EtOH and NMF with the carbonyl nuclei would enhance the resonance stabilization in the vinyl ( $H_2C=CH-$ ) C nuclei in the monomer, which can decrease the electron density in the vinyl group of the monomer. This change in electron density would increase the reactivity of macroradicals, eventually enabling stable chain growth during the polymerization procedure<sup>[12]</sup> (Figure 2C).

We then measured the molecular weights of the synthesized polymer chains in four solvents, named Chain<sub>solvent</sub>, after evaporating the solvents in the synthesized pNIPAAm organogels through gel permeation chromatography (GPC) (Figure 2D,E; Table S1, Supporting Information). The measured weight-average molecular weight  $M_w$  of the Chain<sub>solvent</sub> with  $C_m$  of 21 m were exceeding  $10^6$  g mol<sup>-1</sup>, indicating the formation of long polymer chains. Especially, the Chain<sub>NMF</sub> has the longest polymer chains of  $M_w = 4.5 \times 10^6$  g mol<sup>-1</sup>, which result is supported by the affinitive interaction between the NMF and the NIPAAm. Note that in the case of Chain<sub>EtOH</sub>, relatively short chains of  $M_w = 1.4 \times 10^6$  g mol<sup>-1</sup> were formed in spite of their affinitive interactions, which is thought to be due to a frequent chain transfer to solvent dur-

ing polymerization facilitated by the alcohol group (-OH) in EtOH.<sup>[13]</sup>

We conducted the uniaxial tensile tests for Gel<sub>solvent</sub> series (Figure 2F). The mechanical properties of Gel<sub>solvent</sub>, such as modulus  $E$ , strength  $\sigma$ , and toughness  $\Gamma$ , follow the tendency of  $M_w$  values of Chain<sub>solvent</sub> (Figure S6, Supporting Information). The Gel<sub>NMF</sub> with the highest  $M_w$  is remarkably robust, which has four times higher  $E$ , 10 times higher  $\sigma$ , and 27 times higher  $\Gamma$  than those values of the conventionally made cross-linked hydrogel synthesized in water (x-Gel<sub>water</sub>). The strong and tough Gel<sub>NMF</sub> can endure severe puncture, while the x-Gel<sub>water</sub> cannot (Figure 2G).

We investigated the origin of mechanical properties of the Gel<sub>solvent</sub> (Figure 2H,I). Since chemical cross-linkers were not added in the synthetic process, the mechanical properties of Gel<sub>solvent</sub> would be solely governed by the internal polymer fraction and the chain entanglements. The swelling ratio  $Q$  of Gel<sub>solvent</sub> after equilibrium in water is maintained, which signifies the existence of physical entanglements in the hydrogel networks (Figure S7, Supporting Information). We quantify the entanglement density of the Gel<sub>solvent</sub> by obtaining the entanglement molecular weight  $M_e$  from the storage modulus  $G'$  and the polymer volume fraction  $\phi$  in the equilibrium state (see Experimental Sections). The Gel<sub>NMF</sub> has the lowest  $M_e = 2.7 \times 10^4$  g mol<sup>-1</sup> compared to Gel<sub>DMSO</sub> of  $4.4 \times 10^4$  g mol<sup>-1</sup>, Gel<sub>DMF</sub> of  $5.7 \times 10^4$  g mol<sup>-1</sup>, and Gel<sub>EtOH</sub> of  $1.5 \times 10^5$  g mol<sup>-1</sup>, respectively. Since the  $M_e$  indicates the molecular weight between each entanglement, the lowest  $M_e$  value for Gel<sub>NMF</sub> indicates more entanglements exist in a single polymer strand in the Gel<sub>NMF</sub> than other hydrogels. The  $M_e$  values for Gel<sub>solvent</sub> follow the relation  $M_e \propto \phi^{-4/3}$ , which tendency appears in the linear entangled polymer solution, serving as additional evidence that the Gel<sub>solvent</sub> is a physical gel.<sup>[14]</sup> Conversely, the x-Gel<sub>water</sub> deviates from the tendency due to the presence of rich chemical cross-links. Thus, the deviation of mechanical property in the Gel<sub>solvent</sub> originates from the difference in the internal chain entanglement density. The  $M_e$  values of Gel<sub>solvent</sub> follow the tendency of their  $M_w$  values, which indicates that the formation of longer polymer chains causes more entanglements between the chains during polymerization (Figure 2J).

Since the hydrogels were formed without chemical cross-linkers, the unentangled polymer chains can diffuse out during the solvent exchange process (Figure 2K). We synthesized the organogels and evaporated the organic solvents, and measured the weight of dry polymers  $W_b$ , while measuring the weight of the dried hydrogels after equilibrium swelling  $W_a$ . The weight ratio  $W_a/W_b$  indicates an entangled chain fraction of Gel<sub>solvent</sub>, which was the highest for Gel<sub>NMF</sub>, meaning the most abundant existence of chain entanglements. The entangled chain fraction of Gel<sub>solvent</sub> followed the order of their  $M_e$  values and determined

x-Gel<sub>water</sub> with  $C_m$  of 1.8 m. Data for Gel<sub>EtOH</sub> is unavailable because the gel is too weak to measure. G) Photographs of puncturing test for x-Gel<sub>water</sub> and Gel<sub>NMF</sub>, respectively. Scale bar = 1 cm. H) The storage modulus  $G'$  (filled symbols) and the loss factor  $\tan \delta$  (open symbols) of Gel<sub>solvent</sub> as a function of frequency. The gray triangles are those values of crosslinked hydrogel synthesized in water (x-Gel<sub>water</sub>). I) The entanglement molecular weight  $M_e$  of Gel<sub>solvent</sub> and x-Gel<sub>water</sub> as a function of polymer fraction  $\phi$ . The inset shows the physical meaning of the  $M_e$ . The dashed line indicates  $M_e \approx \phi^{-4/3}$  fit. J) The  $M_e$  of Gel<sub>solvent</sub> as function of  $M_w$  of Gel<sub>solvent</sub>. The dashed line indicates a linear fit. K) Entangled chain fraction  $W_a/W_b$  of the Gel<sub>solvent</sub>. The upper scheme shows the process for measurement of the entangled chain fraction. Values represent the mean and standard deviation ( $n = 3$ ). L) Photographs and scanning electron microscope (SEM) images of Gel<sub>solvent</sub>. Scale bar = 100  $\mu$ m.

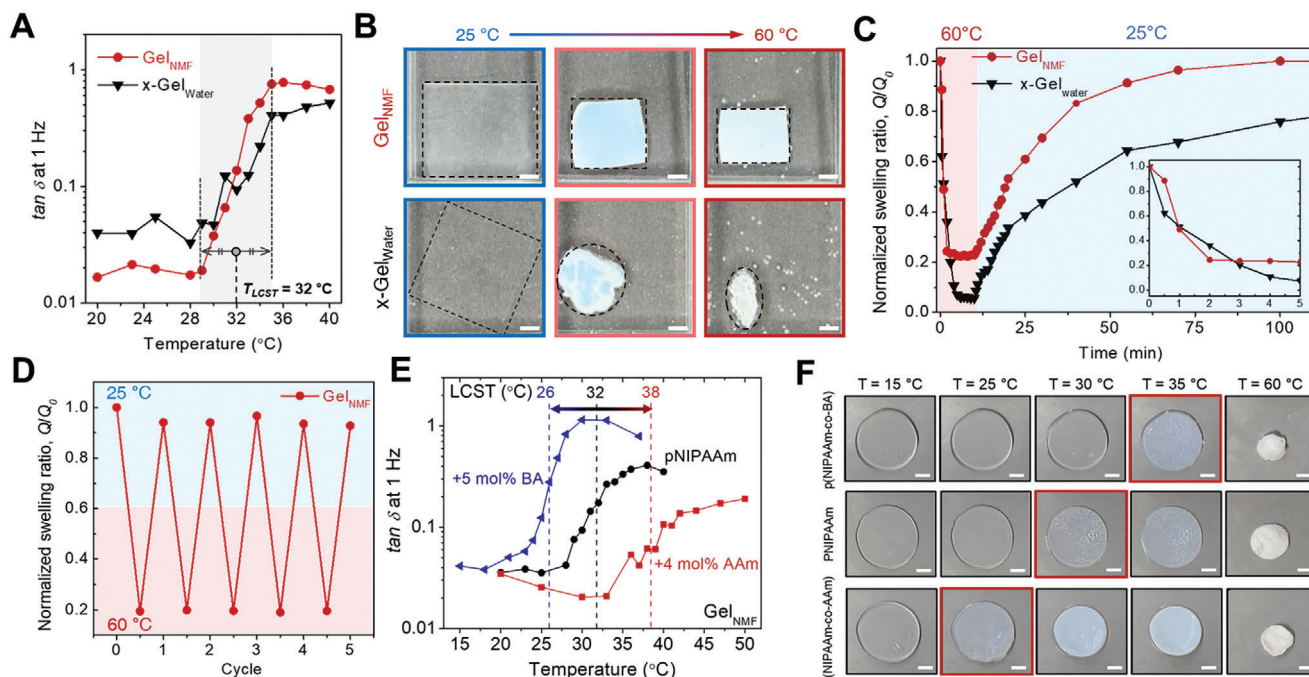


**Figure 3.** LCST behavior of the pNIPAAm hydrogels. A)  $\tan \delta$  at 1 Hz of  $\text{Gel}_{\text{NMF}}$  and  $\text{x-Gel}_{\text{water}}$  as a function of temperature. Lower critical solution temperature (LCST) was defined by the middle of the two points where a significant change of  $\tan \delta$  starts and ends. The LCST of both hydrogels is 32 °C. B) Comparison of the deswelling behavior of  $\text{Gel}_{\text{NMF}}$  and  $\text{x-Gel}_{\text{water}}$  upon increasing temperature above LCST. Scale bar = 5 mm. C) Time-dependent deswelling (at 60 °C, red region) and re-swelling (at 25 °C, blue region) ratios of  $\text{Gel}_{\text{NMF}}$  and  $\text{x-Gel}_{\text{water}}$ . The inset graph is the expanded view of initial deswelling curves. D) Reversible transition behaviors of  $\text{Gel}_{\text{NMF}}$  (circle symbols) and copolymerized  $\text{Gel}_{\text{NMF}}$  with 5 mol.% hydrophobic n-butyl acrylate (BA) monomer (triangle symbols), and 4 mol.% hydrophilic acrylamide (AAm) monomer (rectangular symbols), as a function of temperature. E)  $\tan \delta$  at 1 Hz for  $\text{Gel}_{\text{NMF}}$  (circle symbols) and copolymerized  $\text{Gel}_{\text{NMF}}$  with 5 mol.% hydrophobic n-butyl acrylate (BA) monomer (triangle symbols), and 4 mol.% hydrophilic acrylamide (AAm) monomer (rectangular symbols), as a function of temperature. F) Comparison of the deswelling behavior of LCST-tuned  $\text{Gel}_{\text{NMF}}$  upon increasing temperature. The red boxes highlight the transition onset for the hydrogels. Scale bar = 5 mm.

their  $\phi$  values (Figure S8, Supporting Information). The difference of entanglements and  $\phi$  in the  $\text{Gel}_{\text{solvent}}$  leads to their distinct nanostructures, as revealed in the scanning electron microscope (SEM) images (Figure 2L). The  $\text{Gel}_{\text{EtOH}}$  has a relatively larger pore size, whereas the  $\text{Gel}_{\text{NMF}}$  has the most smaller pore sizes.

Overall, in the process of free-radical polymerization upon initiation, the monomers are propagated to form polymer chains, and the chain entanglement between polymer chains would simultaneously begin to sprout. Among diverse good affinity solvents, the NMF solvent can promote stable chain growth from concentrated monomers by carbonyl-affinitive hydrogen bonding, which realizes highly long polymer chain distributions and abundant chain entanglements in the network. When the synthesized organogel is submerged in water for solvent exchange, the entanglements maintain the shape of hydrogels at the equilibrated state and contribute to mechanical properties, resulting in strong and tough physical hydrogels. We named the overall synthetic process as solvent engineering of hydrogels, and the solvent engineering of pNIPAAm hydrogels can be achieved with the particular solvent–NMF.

## 2.2. LCST Behavior of the pNIPAAm Hydrogels

The solvent engineering strategy to pNIPAAm hydrogels can enhance their mechanical properties without other additional con-

stituents. Hence, the LCST of pNIPAAm hydrogels is not affected (Figure 3A). We measured the LCST of pNIPAAm hydrogels by determining it as a midpoint between the start and end points of notable shifts in rheological loss factor  $\tan \delta$ . Both  $\text{x-Gel}_{\text{water}}$  and  $\text{Gel}_{\text{NMF}}$  exhibit the LCST at 32 °C, however, their responses during transition were different (Figure 3B). The  $\text{x-Gel}_{\text{water}}$  displayed non-isotropic deswelling and surface bubble formation, whereas the  $\text{Gel}_{\text{NMF}}$  deswelled isotropically without bubble formation.<sup>[15]</sup> The deswelling and swelling rate was measured upon subsequent immersion into 60 °C and 25 °C water bath (Figure 3C). The  $\text{Gel}_{\text{NMF}}$  exhibited lower contraction ratio while faster deswelling rate than the  $\text{x-Gel}_{\text{water}}$ , which arises from its higher polymer fraction. The higher polymer fraction in the  $\text{Gel}_{\text{NMF}}$  underwent less water diffusion upon transition, which leads to a lower contraction ratio but faster deswelling rate. Although the  $\text{Gel}_{\text{NMF}}$  consists of linear chains without chemical cross-links, it enables reversible swelling and deswelling during multiple transitions due to its highly long chain length and the resultant abundant entanglements (Figure 3D).

The solvent engineering method basically does not alter the LCST but can modulate it on purpose. The addition of small amount of hydrophilic or hydrophobic monomer results in the desirable change in the LCST (Figure 3E; Figure S9, Supporting Information). Copolymerization with a certain amount of hydrophobic butyl acrylate (BA) from 3 mol.% to 5 mol.% compared to NIPAAm leads to the decrease of LCST of the  $\text{Gel}_{\text{NMF}}$

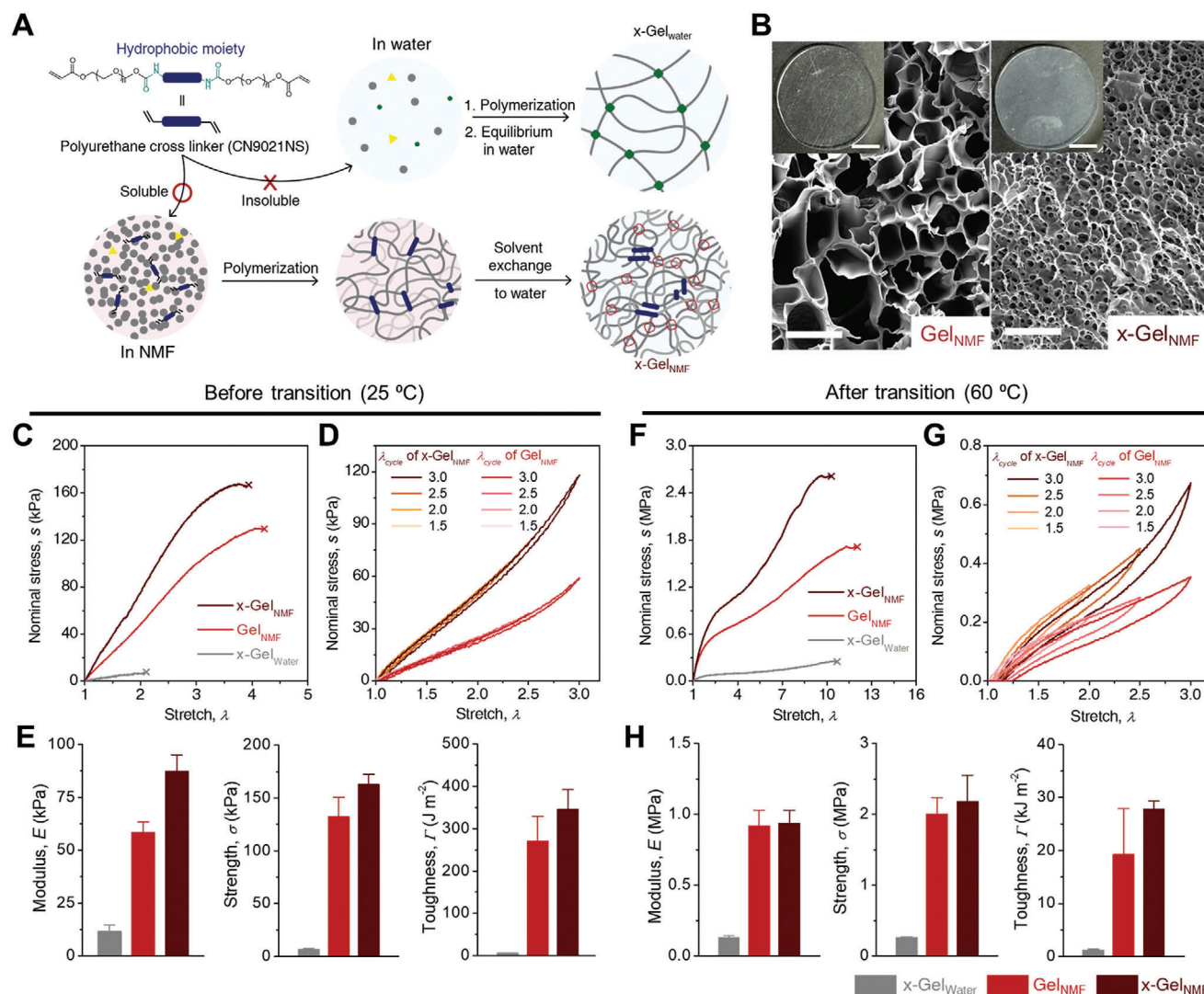


**Figure 4.** Hydrophobic crosslinking strategy for enhancing mechanical properties of the pNIPAAm hydrogels. A) Schematic of hydrophobic crosslinking of  $\text{Gel}_{\text{NMF}}$  by water-insoluble polyurethane crosslinker (CN9021NS) via solvent engineering ( $\text{x-Gel}_{\text{NMF}}$ ). B) SEM images of  $\text{Gel}_{\text{NMF}}$  (left) and  $\text{x-Gel}_{\text{NMF}}$  (right), where the inset photographs show the appearance of each gel. Scale bars in the SEM images and the insets are 50  $\mu\text{m}$  and 5 mm, respectively. C, F) Uniaxial stress-stretch curves of the hydrogels before transition (25 °C) (C) and after transition (60 °C) (F). D, G) Tensile loading-unloading curves of the  $\text{Gel}_{\text{NMF}}$  and  $\text{x-Gel}_{\text{NMF}}$  with increasing stretch from 1.5 to 3 before (D) and after (G) transition. E, H) Young's modulus  $E$ , tensile strength  $\sigma$ , and fracture toughness  $\Gamma$  of the hydrogels before (E) and after transition (H). Values in (E) and (H) represent the mean and standard deviation ( $n = 3$ ).

from 32 °C to 28 °C and 26 °C, respectively. In the same manner, copolymerization with a small amount of hydrophilic acrylamide (AAm) from 2 mol.% to 4 mol.% leads to the increase of LCST of the  $\text{Gel}_{\text{NMF}}$  from 32 °C to 34 °C and 38 °C, respectively. The clear difference of transition temperature can be seen in the series of LCST tuned hydrogels (Figure 3F). Cloudy change and volume shrinkage occur in the hydrophobic p(NIPAAm-co-BA) hydrogel earlier and the hydrophilic p(NIPAAm-co-AAm) later, as the temperatures increases from 15 °C to 60 °C. Consequently, the copolymerization of pNIPAAm hydrogels with solvent engineering can change the LCST of hydrogels while maintaining the contraction ratio and overall mechanical properties.

### 2.3. Enhancing Mechanical Properties Via Hydrophobic cross-linking Strategy

One of the features of solvent engineering is that we do not use the water as an initial solvent for synthesizing hydrogels. On that account, we introduced a polyurethane oligomeric crosslinker (CN9021NS), which has been used for designing robust elastomers.<sup>[16]</sup> While the polyurethane cross-linker has not been used in synthesizing hydrogels due to its insolubility in water, our solvent system allows to use it for enhancing mechanical properties of  $\text{Gel}_{\text{NMF}}$  (Figure 4A; Figure S10, Supporting Information). First, we optimized the mechanical properties of  $\text{Gel}_{\text{NMF}}$  with  $C_m$  to 32 m and all subsequent syntheses were conducted at



this concentration (Figure S11, Supporting Information). Then, we synthesized the cross-linked Gel<sub>NMF</sub> (x-Gel<sub>NMF</sub>) with adding 1 wt.% of the hydrophobic cross-linker. When undergoing solvent exchange in the x-Gel<sub>NMF</sub>, the effect of cross-linker becomes apparent as it induces phase separation that makes the hydrogel slightly cloudy. The phase separation caused a significant reduction in the pore size of hydrogels, typically observed in hydrophobic phase-separated hydrogels<sup>[17]</sup> (Figure 4B). The hydrophobicity of the cross-linker leads to a higher  $\phi$  and a faster deswelling rate (Figures S12 and S13, Supporting Information). Still, the presence of cross-linker does not alter the LCST of hydrogel, possibly due to the small amount of the cross-linker (Figure S14, Supporting Information).

We conducted uniaxial stress-stretch tests of the pNIPAAm hydrogels in different temperatures (before transition at 25 °C and after transition at 60 °C, respectively) (Figure 4C,F). Note that the Gel<sub>NMF</sub> still exhibited superior mechanical properties over other Gel<sub>solvent</sub> series or x-Gel<sub>water</sub> after transition (Figure S15, Supporting Information). Young's modulus  $E$ , tensile strength  $\sigma$ , and toughness  $\Gamma$  of the solvent-engineered pNIPAAm hydrogels before transition (Figure 4E) and after transition (Figure 4H) showed remarkable mechanical enhancement compared to the conventional x-Gel<sub>water</sub>. The  $E$ ,  $\sigma$ , and  $\Gamma$  of the Gel<sub>NMF</sub> in 25 °C were 58 kPa and 132 kPa, and 272 J m<sup>-2</sup>, which were respectively 5 times, 19 times and 43 times higher than those of x-Gel<sub>water</sub>. The x-Gel<sub>NMF</sub> has the  $E$ ,  $\sigma$ , and  $\Gamma$  of 87 kPa and 162 kPa and 346 J m<sup>-2</sup> in 25 °C, which were respectively 1.5 times, 1.2 times, and 1.3 times enhanced properties than those of uncross-linked Gel<sub>NMF</sub>. Solvent-engineered pNIPAAm hydrogels exhibited a remarkable elasticity (Figure 4D). Under the loading-unloading tensile test with increasing stretch  $\lambda$  from 1.5 to 3, the mechanical hysteresis for both the Gel<sub>NMF</sub> and the x-Gel<sub>NMF</sub> were negligible. More specifically, the dissipated energy during loading and unloading, represented by the ratio of the area between the loading and unloading curves to the area under the loading curve, is under 1%. Such highly elasticity properties are similar to those appearing in highly entangled hydrogels.<sup>[14b,18]</sup> While after transition, as the water in the hydrogels exits, the decreased water content in hydrogels increases the interchain friction, which results in slightly increased hysteresis to  $\approx 19\%$  (Figure 4G and Figures S16, S17, and Table S3, Supporting Information). The increased polymer fraction leads to an overall improvement of mechanical properties, where the  $E$ ,  $\sigma$ , and  $\Gamma$  of the Gel<sub>NMF</sub> after transition were 0.9 MPa and 2.0 MPa, and 19.3 kJ m<sup>-2</sup>, which were respectively seven times, eight times, and 15 times higher than those of x-Gel<sub>water</sub>. The x-Gel<sub>NMF</sub> has the  $E$ ,  $\sigma$ , and  $\Gamma$  of 0.9 MPa and 2.2 MPa, and 27.8 kJ m<sup>-2</sup>, where those values were similar to those of uncross-linked Gel<sub>NMF</sub>. Since the most of water exits from the hydrogels after transition, the polymer fraction is similar for the Gel<sub>NMF</sub> and the x-Gel<sub>NMF</sub>, where the mechanical enhancement by the cross-linking after transition is relatively small compared to that before transition. The solvent-engineered pNIPAAm hydrogel is mechanically robust, where it can bear the lift 10,000 times of its own weight after transition (Movie S2, Supporting Information). Such high mechanical properties with low hysteresis of the pNIPAAm hydrogels both before and after transition have not been simultaneously achieved, even with a form of single component hydrogels, to the best of our knowledge.

## 2.4. Actuation Performance of the Hydrogel and Application

We compared the actuation performance of the pNIPAAm hydrogels (Figure 5). To quantify the contraction strength  $\sigma_c$ , each end of hydrogel samples was fixed, and hot water (60 °C) was poured over, while the contraction stress generated over time was measured (Figure 5A). Over the same duration, the x-Gel<sub>NMF</sub> and the Gel<sub>NMF</sub> generated the  $\sigma_c$  of 47.5 kPa and 34 kPa, respectively. These values are respectively 16 times and 11 times higher than that of x-Gel<sub>water</sub> of 3 kPa (Figure 5B). When comparing the actuation speed, defined by the reciprocal of time to reach 90% of its maximum strength  $t_{90\%}^{-1}$ , the x-Gel<sub>NMF</sub> showed the fastest actuation, which takes  $\approx 90$  s to actuate (Figure 5C). These values are 3.7 times faster than that of the x-Gel<sub>water</sub>. The x-Gel<sub>NMF</sub> produces the fastest and greatest actuation stress, which can be possibly achieved by its largest polymer fraction and minimal water content to exit. The x-Gel<sub>NMF</sub> consistently generates similar  $\sigma_c$  through repeated releases at room temperature (25 °C) and actuations (60 °C) (Figure 5D).

To quantify the specific work capacity  $W$  of the pNIPAAm hydrogels, we investigated the load-stroke relationship of the hydrogel actuation. By gradually increasing the mass of weight to the hydrogel samples of a uniform size, we measured the distance they can lift (Figures S18–S20, Supporting Information). The x-Gel<sub>NMF</sub> can lift weights up to 100 times its own mass with an actuation strain of 48%, 200 times its mass with a strain of 24%, and even 300 times its mass with a strain of 11% (Figure 5E; Figures S18–S20, Supporting Information). Furthermore, the high fracture toughness of x-Gel<sub>NMF</sub> enables the lift of weights up to 150 times its own mass with an actuation strain of 23.8% even with a notch (Figure 5F; Movie S3, Supporting Information). We calculated the  $W$  by dividing the area under the load-stroke curve by the volume of samples. We could not measure the force of x-Gel<sub>water</sub> at zero stoke due to its weakness, leading us to estimate the  $W$  using extrapolated values (Figure 5G). The calculated  $W$  for x-Gel<sub>NMF</sub> and Gel<sub>NMF</sub> were 41 kJ m<sup>-3</sup> and 33 kJ m<sup>-3</sup>, which values are 6.8 times and 5.5 times higher than that of x-Gel<sub>water</sub> (6 kJ m<sup>-3</sup>), respectively (Figure 5H).

The actuation of solvent-engineered pNIPAAm hydrogels even outperforms other pNIPAAm-based contractile hydrogel actuations<sup>[2a,b,9a,11,19]</sup> (Figure 5I; Table S2, Supporting Information). The significant enhancement of work capacity  $W$  during actuation was achieved by the gels, which originates from the large actuation strain without compensation of actuation strength compared to other strategies. Since the actuation performance of pNIPAAm hydrogels has been developed by adding additional networks, the decreased ratio of pNIPAAm network often caused a reduction of the actuation strain. On the other hand, the solvent engineering enables the synthesis of strong and tough pNIPAAm hydrogels by themselves, which facilitates both high actuation strength and strain, exhibiting five times higher work capacity than that of biological muscles.<sup>[20]</sup>

The simplicity of solvent engineering strategy would facilitate the synthesis of robust pNIPAAm hydrogels for various applications. As a proof of concept, we synthesized the solvent-engineered pNIPAAm hydrogel nanocomposites with the incorporation of gold nanoparticles (AuNPs) having photothermal properties (AuNP@x-Gel<sub>NMF</sub>) (Figure S21, Supporting Information). The AuNP@x-Gel<sub>NMF</sub> exhibited the significant

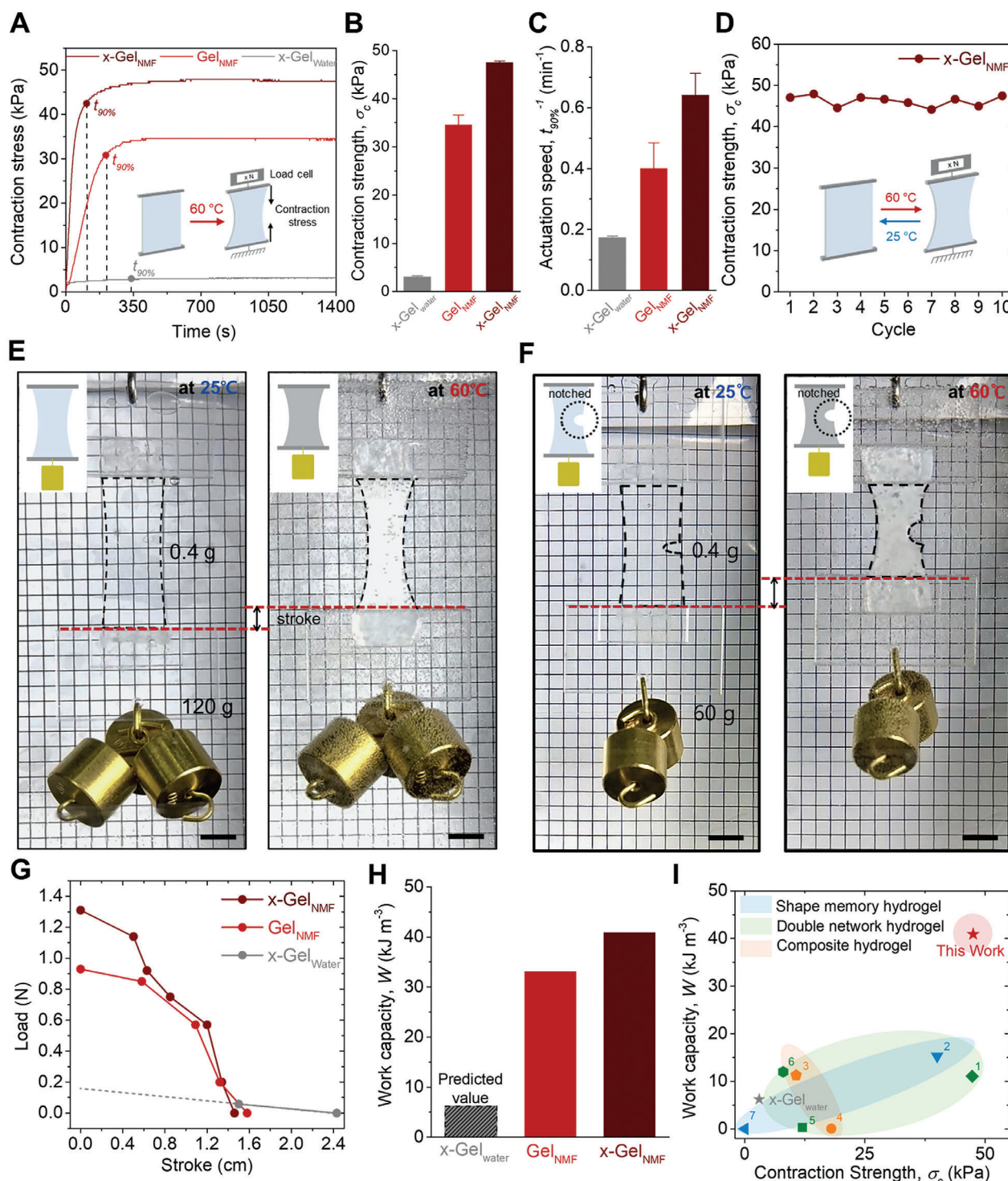


**Figure 5.** Actuation performance of the hydrogels. A) Contraction stress of the hydrogels as a function of time. Inset schematic shows the process of the contraction stress measurement. The points of  $t_{90\%}$  in each graph indicate the time when 90% of contraction strength is achieved. B,C) Contraction strength  $\sigma_c$  (B) and contraction speed  $t_{90\%}^{-1}$  (C) for the hydrogels. Values represent the mean and standard deviation ( $n = 3$ ). D) Reversible actuation of the x-Gel<sub>NMF</sub>. The actuation and the release temperatures are 60 °C and 25 °C, respectively. E,F) Photographs of the contractile actuation of x-Gel<sub>NMF</sub> without E) and with a notch F). The notch-to-width ratio is 1/3. Mass of hydrogels is 0.4 g, and mass of weights is 120 g (left) and 60 g (right), respectively. Scale bar = 1 cm. G) Load versus stroke curves in actuation process of the hydrogels. The load is a sum of that of the weight and the acrylic sheet, adjusted for the buoyancy effect of both. The gray dashed line is the extrapolated line, since the zero-stroke load of x-Gel<sub>Water</sub> is unable to measure due to the weakness of the gel. H) Work capacity  $W$  of the hydrogels.  $W$  of x-Gel<sub>Water</sub> is a predicted value. I) A comparison of the  $W$  and  $\sigma_c$  of solvent-engineered x-Gel<sub>NMF</sub> with conventional and other pNIPAAm hydrogel-based actuations.



enhancement in mechanical properties with 35 times higher  $E$  and 30 times higher  $\sigma$  than those of the conventionally made one in aqueous solution ( $\text{AuNP}@x\text{-Gel}_{\text{water}}$ ). We can demonstrate a light-driven actuation of the  $\text{AuNP}$ -pNIPAAm hydrogel nanocomposites, where the distinct actuation response was observed under irradiation; the solvent-engineered one can actuate to bend itself by irradiation, while the conventionally made one cannot, due to their distinct mechanical properties (Movie S4, Supporting Information).

### 3. Conclusion

The proposed solvent engineering strategy has unveiled the affinitive solvent for the NIPAAm monomer, which greatly improves the mechanical and actuation performances of the pNIPAAm hydrogels. A proper solvent replacement in polymerization can lead to extremely long and entangled pNIPAAm polymer chains, where the simplicity of the synthetic process could be easily harmonized to design robust pNIPAAm-based applications. Considering that the solvent effect during polymerization is distinct, it would be important for other types of functional hydrogels or even elastomers to find their own affinitive solvents, for improving their mechanical properties. We anticipate that the presented strategy here will solidly expand the scope of stimuli-responsive hydrogel-based applications.

### 4. Experimental Section

**Materials:** *N*-Isopropylacrylamide (NIPAAm,  $\geq 99\%$ ), *N*-methylformamide (NMF), dimethyl sulfoxide (DMSO), *N,N*-dimethylformamide (DMF), ethanol (EtOH), *N,N*-methylenebisacrylamide (MBAAm), acrylamide (AAm), butyl acrylate (BA), gold(III) chloride trihydrate, and sodium citrate dihydrate were purchased from Sigma-Aldrich. 2-Hydroxy-2-methylpropiophenone (HMPP) and *N,N*-Bis(acryloyl)cystamine were purchased from TCI chemicals. Water-insoluble urethane cross-linker (CN9021NS) was purchased from Sartomer Americas. All chemicals were used as received, while DMSO and DMF were used after dried by 4 Å molecular sieves.

**Preparation of pNIPAAm Physical Hydrogels ( $\text{Gel}_{\text{solvent}}$ ):** NIPAAm (2.4 g) and organic solvents (1 g of NMF, DMSO, DMF, and EtOH) were mixed to make a monomer solution. A HMPP initiator solution (0.05 M) was prepared with each solvent. The initiator solution (5  $\mu\text{L}$ ) was added to the monomer solutions and stirred for 30 min. The precursor solution was injected to customized molds, consisting of two Teflon-taped glass slide with 400  $\mu\text{m}$  thick stacked PET film spacer. Then, the polymerization was carried out under 365 nm ultraviolet (UV) irradiation (CL-1000L, UVP) for 12 h. After that, the stiff organogels were obtained and submerged in fresh water for solvent exchange more than 3 days to swell to equilibrium. During swelling, the water was exchanged every 3 h.

For conventional pNIPAAm hydrogels, 2 g of NIPAAm was dissolved in 10 mL of water to make a monomer solution. A MBAAm cross-linker solution (0.1 M) was prepared with water. The cross-linker solution (0.25 mL) and the initiator solution (5  $\mu\text{L}$ ) were added to the monomer solution and stirred for 30 min. The precursor solution was injected to the customized molds and immersed in cold water bath. Polymerization was carried out under 365 nm of UV irradiation for 2 h. After that, the obtained hydrogel was submerged in fresh water more than 3 days to swell to equilibrium. During the swelling, the water was changed every 3 h.

**Preparation of p(NIPAAm-co-BA) and p(NIPAAm-co-AAm) Hydrogel:** NIPAAm (3.6 g) was dissolved 1 mL of NMF to make a monomer solution. BA (3 or 5 mol.%) and AAm (2 or 4 mol.%) were added to the monomer solution, respectively. The initiator solution (5  $\mu\text{L}$ ) was added to

the monomer solutions and stirred for 30 min. The subsequent process was carried out in the same manner of preparing  $\text{Gel}_{\text{solvent}}$ .

**Preparation of  $x\text{-Gel}_{\text{NMF}}$ :** CN9021NS (0.3 g) and NMF (10 mL) were mixed to make a hydrophobic cross-linker solution. NIPAAm (3.6 g), the hydrophobic cross-linker solution (1 mL), and the initiator solution (5  $\mu\text{L}$ ) were mixed and stirred for 30 min. The subsequent process was carried out in the same manner of preparing  $\text{Gel}_{\text{solvent}}$ .

**Preparation of  $\text{AuNP}@x\text{-Gel}_{\text{NMF}}$  and  $\text{AuNP}@x\text{-Gel}_{\text{water}}$ :** Gold nanoparticles (AuNPs) were synthesized according to literature procedure.<sup>[28]</sup> Gold(III) chloride trihydrate (0.17 g) was added to 250 mL of water to make a seed solution. The seed solution was then heated to its boiling point with a stirring speed of 400 rpm. 20 mL of 1 wt.% sodium citrate dihydrate solution was then added into the seed solution followed by an immediate increase of the stirring speed to 800 rpm. The solution was left to boil for another 6 min, after which the hotplate was switched off. After cooling, the solution was centrifuged at 6000 rpm, and the AuNPs were collected.

For making  $\text{AuNP}@x\text{-Gel}_{\text{NMF}}$ , NIPAAm (2.4 g) was dissolved in 1 mL of NMF to make a monomer solution. AuNP (24 mg), *N,N*-bis(acryloyl)cystamine (5 mg) and the initiator solution (5  $\mu\text{L}$ ) were added to the monomer solution and stirred for 30 min. The subsequent process was carried out in the same manner of preparing  $\text{Gel}_{\text{solvent}}$ .

For making  $\text{AuNP}@x\text{-Gel}_{\text{water}}$ , NIPAAm (2 g) was dissolved in 10 mL of water to make a monomer solution. AuNP (20 mg), *N,N*-bis(acryloyl)cystamine (4 mg) and the initiator solution (5  $\mu\text{L}$ ) were added to the monomer solution and stirred for 30 min. The subsequent process was carried out in the same manner of preparing  $\text{Gel}_{\text{solvent}}$ .

**Solubility Test:** For the characterization of the solubility of the NIPAAm monomer, the monomer was dissolved in 1 g of diverse solvent at 40 °C with magnetic stirring. The solubility limit was considered the concentration at which the monomer began to precipitate.

**Nuclear Magnetic Resonance (NMR) Characterizations:** For the characterization of  $^{13}\text{C}$ -NMR, NIPAAm monomer ( $C_m = 5$  M) was dissolved in organic solvents (NMF, DMSO, DMF, and EtOH). Then, the monomer solutions were loaded to coaxial insert NMR tube and  $\text{CDCl}_3$  was load to outer tube to measure.  $^{13}\text{C}$ -NMR spectra were acquired by AVANCE NEO 400, Bruker spectrometer at a  $^{13}\text{C}$ -NMR frequency of 400 MHz, using chemical shift of  $^{13}\text{C}$ -nucleus in NIPAAm monomer dissolved in  $\text{CDCl}_3$  ( $C_m = 5$  M) as a reference. For the characterization by  $^1\text{H}$ -NMR, the as-prepared  $\text{Gel}_{\text{solvent}}$  was dissolved in  $\text{CDCl}_3$  (ca. 1 wt.%) under stirring at room temperature overnight, and then used to investigate  $^1\text{H}$ -NMR spectra. Monomer conversion was confirmed by the  $^1\text{H}$ -NMR spectra.

**Fourier Transform Infrared (FT-IR) Characterizations:** FT-IR spectrometer (Nicolet iS50, Thermo Fisher Scientific) was used to conduct the FT-IR spectroscopic analysis of the NIPAAm monomer solutions in organic solvents (NMF, DMSO, DMF, and EtOH) with  $C_m$  of 5 M.

**Gel Permeation Chromatography (GPC) Characterizations:** For the characterization of molecular weight distribution, the as-prepared stiff organogels with various solvents were kept on 65 °C oven under vacuum to remove unreacted monomers and organic solvents for 7 days, until constant weight was observed. Then, 2 mg of the polymers were dissolved in 1 mL of DMF with lithium bromide (LiBr) as an eluent (20 mM), under stirring at room temperature overnight. The average molecular weight ( $M_n$ ,  $M_w$ ,  $M_z$ ) and the polydispersity index (PDI) of obtained pNIPAAm polymers were determined by gel permeation chromatography (GPC) using the DMF solution.

**Mechanical Tests for Hydrogels:** All the mechanical tests were conducted in a water chamber, which was made of acrylic plates. The grippers were made of acrylic sheets. The hydrogel samples were cut into a rectangular shape with 10 mm x 30 mm (5 mm x 30 mm for after transition samples), glued with the grippers using Krazy glue, and loaded to a universal testing machine (Instron 3343) with a 50 N load cell. The gauge length of all specimens was fixed to 3 mm. The modulus was measured from the initial slope of the stress-stretch curve. The stretch rates were kept constant at 4  $\text{min}^{-1}$  unless specified. Tensile loading-unloading of the hydrogels were conducted with the universal testing machine, with varying applied stretch  $\lambda_{\text{app}}$  from 1.5 to 3.0. Fracture test specimens were prepared by half-notched in the middle point of the specimens, and the fracture toughness  $\Gamma$  is defined as the work done by unnotched sample

until the critical distance  $d_c$  of notched sample,  $U(d_c)$ , divided by the width  $w_0$  and the thickness  $t_0$  of the unnotched sample (Figure S22, Supporting information). Mechanical tests were performed at room temperature (25 °C) and 60 °C for before transition and after transition, respectively. Detailed measurement setups are illustrated in Figure S23. Note that the buoyancy effect during measurement is negligible (Figure S24, Supporting information).

**Rheological Properties Measurement:** The viscoelastic behavior of the hydrogels was investigated by a rheometer (DHR-2, TA Instruments). The hydrogel samples were cut into disc-shape specimens with the thickness of  $\approx 1.6$  mm and the diameter of 20 mm. Rheological frequency sweeps, from 100 rad s<sup>-1</sup> to 0.1 rad s<sup>-1</sup> with 0.1% of applied shear strain in parallel plates geometry, were performed over a wide range of temperature from 15 °C to 50 °C. The rheological loss factor  $\tan \delta$  is defined as the ratio of loss modulus  $G''$  to the storage modulus  $G'$  at 1 Hz. Lower critical solution temperature (LCST) of the hydrogels was defined by the middle of the two points where a significant change of  $\tan \delta$  starts and ends. The materials were submerged in water during the experiment. Note that the absolute values of  $G'$  and  $G''$  was fluctuated when changing temperature due to volumetric contraction of hydrogels, however, the values of  $\tan \delta$  show coherent tendency, where could be determined the LCST of hydrogels from those values.

For estimating the entanglement molecular weight  $M_e$ , The physical hydrogels were assumed as affine network model and the physical entanglement as an analogous cross-link.<sup>[14a]</sup> The entanglement density can be estimated with  $G' = \varphi NkT$ , where  $\varphi$  is the polymer fraction in a gel,  $N$  is the number density of entanglement strands, and  $kT$  is thermal energy in a given temperature. Given that the occupied volume of an entanglement strand is the reciprocal of  $N$ , then  $M_e = \rho N_A N^{-1}$ , where  $\rho$  is the density of the polymer and  $N_A$  is Avogadro's number. The  $M_e$  of hydrogels were estimated from  $G'$  and  $\varphi$  by substituting  $\rho$  and  $T$  to 1.1 and 298 K, respectively.

**Swelling and De-Swelling Test:** The hydrogel samples were cut into a rectangular shape with 15 mm x 15 mm. Then, the hydrogel samples were soaked into the hot water chamber (60 °C) and the weight of the hydrogels was measured over time. When there was no further change in the weight of the hydrogels, samples were soaked again into the room temperature water chamber (25 °C) and the weight of hydrogels were measured over time. For the reversible transition test, hydrogel samples were immersed in the hot water chamber for a day and their weights were measured. Subsequently, the samples were immersed again in the tepid water chamber for a day and their weights were measured. This cycle was repeated 5 times.

Normalized swelling ratio  $Q/Q_0$  was measured, as defined by the following equation:

$$\frac{Q}{Q_0} = \frac{W_t - W_i}{W_i} \quad (1)$$

where  $W_i$  and  $W_t$  are the weights of the initial hydrogel samples and the weights at a certain equilibrium, respectively.

**Measurement of Contraction Force and Work Capacity:** All the actuation tests were conducted in the water chamber. The grippers were made of acrylic sheets. The hydrogel samples were cut into a rectangular shape with 20 mm x 35 mm, glued with the grippers using Krazy glue, and loaded to a force gauge sensor (MARK-10, series 5). The gauge length of all specimens was fixed to 25 mm. For the contraction force measurement, hot water (60 °C) was poured into the chamber and the contraction force was recorded for 15 min. Contraction strength  $\sigma_c$  is defined as the contraction force divided by the width  $w_0$  and the thickness  $t_0$  of the samples.

For the reversible actuation test, the measured samples were submerged in room temperature fresh water for a day then measured the  $\sigma_c$  again. This procedure was repeated for 10 times. Detailed measurement setups are illustrated in Figure S23 (Supporting Information).

The load-stroke relationship was determined by measuring the stroke with gradually increasing the load of weight hanging from the sample (from 0 to 140 g). Then, the temperature of water chamber was raised to 60 °C. The lifting stroke during actuation was measured with recorded videos. Work capacity  $W$  is defined by the area under the plotted load-

stroke graph divided by the volume ( $w_0 \times t_0 \times l_0$ ) of the samples. Detailed measurement setups are illustrated in Figure S23 (Supporting Information).

**Characterization for AuNP@x-Gel<sub>NMF</sub> and AuNP@x-Gel<sub>water</sub>:** To confirm the formation of AuNPs in the hydrogels, the absorbance spectra were measured by a UV-Vis spectrometer (Cary 60 UV-Vis, Agilent Technologies). The obtained hydrogel composites were cut into a rectangular shape with 5 mm x 25 mm for the actuation test. Then, the hydrogel samples were submerged in water chamber. An infrared light source (PSU-H-LED) was positioned 3 cm above the sample, and the light was turned on for 20 s. Subsequently, the bending angle of the hydrogel was measured.

## Supporting Information

Supporting Information is available from the Wiley Online Library or from the author.

## Acknowledgements

This work was supported by a National Research Foundation of Korea (NRF) grant funded by the Korean Government (No. 2021R1A2C2092737). This work was supported by the Pioneer Research Center Program through the National Research Foundation of Korea funded by the Ministry of Science, ICT & Future Planning (grant no. NRF-2022M3C1A3081211).

## Conflict of Interest

The authors declare no conflict of interest.

## Author Contributions

Y.E.C. and J.-M.P. equally contributed to this work. Y.E.C. conceived the idea. Y.E.C. and J.-M.P. developed materials and methods for the solvent engineering of hydrogels. Y.E.C. and J.-M.P. conducted the solubility test, NMR measurement, and GPC measurement. Y.E.C. and J.-M.P. conducted the mechanical test for hydrogels and interpreted the results. Y.E.C., J.-M.P., and W.J.S. conducted the mechanical test for the urethane cross-linked hydrogels and interpreted the results. Y.E.C. and J.-M.P. designed the schematics and Y.E.C., J.-M.P., and M.G.L. conducted movie recordings for the experiments. Y.E.C., J.-M.P., M.G.L., and J.-Y.S. analyzed the results. J.-M.P., Y.E.C., and J.-Y.S. wrote the manuscript with the input from all authors. J.-Y.S. supervised the study.

## Data Availability Statement

The data that support the findings of this study are available from the corresponding author upon reasonable request.

## Keywords

Actuation, Hydrogel synthesis, poly(N-isopropylacrylamide), Solvent engineering, Stimuli-responsive hydrogels

Received: April 29, 2024

Revised: June 23, 2024

Published online: July 22, 2024

[1] M. A. Haq, Y. Su, D. Wang, *Mater. Sci. Eng. C Mater. Biol. Appl.* **2017**, 70, 842.

- [2] a) L. Zhang, H. Yan, J. Zhou, Z. Zhao, J. Huang, L. Chen, Y. Ru, M. Liu, *Adv. Mater.* **2023**, 35, 2202193; b) M. Hauck, L. M. Saure, B. Zeller-Plumhoff, S. Kaps, J. Hammel, C. Mohr, L. Rieck, A. S. Nia, X. Feng, N. M. Pugno, R. Adelung, F. Schutt, *Adv. Mater.* **2023**, 35, 2302816; c) Z. Sun, Y. Yamauchi, F. Araoka, Y. S. Kim, J. Bergueiro, Y. Ishida, Y. Ebina, T. Sasaki, T. Hikima, T. Aida, *Angew. Chem. Int. Ed. Engl.* **2018**, 57, 15772; d) F. G. Downs, D. J. Lunn, M. J. Booth, J. B. Sauer, W. J. Ramsay, R. G. Klemperer, C. J. Hawker, H. Bayley, *Nat. Chem.* **2020**, 12, 363; e) C. Ni, D. Chen, X. Wen, B. Jin, Y. He, T. Xie, Q. Zhao, *Nat. Commun.* **2023**, 14, 7672; f) Y. S. Kim, M. Liu, Y. Ishida, Y. Ebina, M. Osada, T. Sasaki, T. Hikima, M. Takata, T. Aida, *Nat. Mater.* **2015**, 14, 1002; g) G. Hou, X. Zhang, F. Du, Y. Wu, X. Zhang, Z. Lei, W. Lu, F. Zhang, G. Yang, H. Wang, Z. Liu, R. Wang, Q. Ge, J. Chen, G. Meng, N. X. Fang, X. Qian, *Nat. Nanotechnol.* **2024**, 19, 77; h) Y. Zhao, C. Xuan, X. Qian, Y. Alsaïd, M. Hua, L. Jin, X. He, *Sci Robot* **2019**, 4; i) Y. Zhao, C. Y. Lo, L. Ruan, C. H. Pi, C. Kim, Y. Alsaïd, I. Frenkel, R. Rico, T. C. Tsao, X. He, *Sci Robot* **2021**, 6.
- [3] a) J. Kim, S. Im, J. H. Kim, S. M. Kim, S. M. Lee, J. Lee, J. P. Im, J. Woo, S. E. Moon, *Adv. Mater.* **2020**, 32, 1905901; b) M. Hippler, E. Blasco, J. Qu, M. Tanaka, C. Barner-Kowollik, M. Wegener, M. Bastmeyer, *Nat. Commun.* **2019**, 10, 232; c) M. Zhang, A. Pal, Z. Zheng, G. Gardi, E. Yildiz, M. Sitti, *Nat. Mater.* **2023**, 22, 1243; d) H. Kim, K. Kim, S. J. Lee, *NPG Asia Mater* **2017**, 9, e445.
- [4] A. K. Mishra, T. J. Wallin, W. Pan, A. Xu, K. Wang, E. P. Giannelis, B. Mazzolai, R. F. Shepherd, *Sci Robot* **2020**, 5.
- [5] X. Qian, Y. Zhao, Y. Alsaïd, X. Wang, M. Hua, T. Galy, H. Gopalakrishna, Y. Yang, J. Cui, N. Liu, M. Marszewski, L. Pilon, H. Jiang, X. He, *Nat. Nanotechnol.* **2019**, 14, 1048.
- [6] Z. Zhu, J. Wang, X. Pei, J. Chen, X. Wei, Y. Liu, P. Xia, Q. Wan, Z. Gu, Y. He, *Sci. Adv.* **2023**, 9, eadh2213.
- [7] a) X. Kuang, Q. Rong, S. Belal, T. Vu, A. M. Lopez Lopez, N. Wang, M. O. Arican, C. E. Garciamendez-Mijares, M. Chen, J. Yao, Y. S. Zhang, *Science* **2023**, 382, 1148; b) B. S. Kim, M. K. Kim, Y. Cho, E. E. Hamed, M. U. Gillette, H. Cha, N. Miljkovic, V. K. Aakalu, K. Kang, K. N. Son, K. M. Schachtschneider, L. B. Schook, C. Hu, G. Popescu, Y. Park, W. C. Ballance, S. Yu, S. G. Im, J. Lee, C. H. Lee, H. Kong, *Sci. Adv.* **2020**, 6.
- [8] a) H. Tian, C. Wang, Y. Chen, L. Zheng, H. Jing, L. Xu, X. Wang, Y. Liu, J. Hao, *Sci. Adv.* **2023**, 9, eadd6950; b) M. Faghih, D. Karnaushenko, Q. A. Besford, C. Becker, R. Ravishankar, D. D. Karnaushenko, G. Cuniberti, A. Fery, O. G. Schmidt, *Adv. Funct. Mater.* **2022**, 32.
- [9] a) Y. W. Kim, D. Y. Kim, J. Y. Sun, *Gels* **2022**, 8; b) L. W. Xia, R. Xie, X. J. Ju, W. Wang, Q. Chen, L. Y. Chu, *Nat. Commun.* **2013**, 4, 2226; c) P. de Almeida, M. Jaspers, S. Vaessen, O. Tagit, G. Portale, A. E. Rowan, P. H. J. Kouwer, *Nat. Commun.* **2019**, 10, 609; d) S. Hu, Y. Fang, C. Liang, M. Turunen, O. Ikkala, H. Zhang, *Nat. Commun.* **2023**, 14, 3717; e) R. Fei, J. T. George, J. Park, A. K. Means, M. A. Grunlan, *Soft Matter* **2013**, 9, 2912.
- [10] J. Wang, L. Lin, Q. Cheng, L. Jiang, *Angew Chem Int Ed Engl* **2012**, 51, 4676.
- [11] M. Hua, D. Wu, S. Wu, Y. Ma, Y. Alsaïd, X. He, *ACS Appl. Mater. Interfaces* **2021**, 13, 12689.
- [12] a) H. Fujihara, K. Yamazaki, Y. Matsubara, M. Yoshihara, T. Maeshima, *J. Macromol. Sci. Part A – Chem.* **1979**, 13, 1081; b) K. Liang, R. A. Hutchinson, *Macromol. Rapid Commun.* **2011**, 32, 1090; c) M. D. Costioli, D. Berdat, R. Freitag, X. André, A. H. E. Müller, *Macromolecules* **2005**, 38, 3630; d) A. Valdebenito, M. V. Encinas, *Polym. Int.* **2010**, 59, 1246; e) S. Beuermann, *Macromolecules* **2004**, 37, 1037; f) S. Beuermann, *Macromol. Rapid Commun.* **2009**, 30, 1066.
- [13] a) J. Loiseau, N. Doërr, J. M. Suau, J. B. Egraz, M. F. Llauro, C. Ladavière, J. Claverie, *Macromolecules* **2003**, 36, 3066; b) A. Matsumoto, Y. Mohri, *J. Polymer Sci. Part A: Polym. Chem.* **1999**, 37, 2803.
- [14] a) M. Rubinstein, R. H. Colby, *Polymer Physics*, Oxford University Press, Oxford, UK **2003**; b) G. Nian, J. Kim, X. Bao, Z. Suo, *Adv. Mater.* **2022**, 34, 2206577.
- [15] K. Kratz, T. Hellweg, W. Eimer, *Polymer* **2001**, 42, 6631.
- [16] a) Z. Peng, Y. Shi, N. Chen, Y. Li, Q. Pei, *Adv. Funct. Mater.* **2020**, 31; b) M. Gao, H. Wu, R. Plamthottam, Z. Xie, Y. Liu, J. Hu, S. Wu, L. Wu, X. He, Q. Pei, *Matter* **2021**, 4, 1962.
- [17] a) G. Zhang, J. Kim, S. Hassan, Z. Suo, *Proc. Natl. Acad. Sci. USA* **2022**, 119, 2203962119; b) G. Zhang, J. Steck, J. Kim, C. H. Ahn, Z. Suo, *Sci. Adv.* **2023**, 9, eadh7742.
- [18] a) C. Norioka, Y. Inamoto, C. Hajime, A. Kawamura, T. Miyata, *NPG Asia Mater* **2021**, 13; b) J. Kim, G. Zhang, M. Shi, Z. Suo, *Science* **2021**, 374, 212.
- [19] a) Z. Jiang, S. M. Seraji, X. Tan, X. Zhang, T. Dinh, M. Mollazade, A. E. Rowan, A. K. Whittaker, P. Song, H. Wang, *Chem. Mater.* **2021**, 33, 7818; b) Y. Ma, M. Hua, S. Wu, Y. Du, X. Pei, X. Zhu, F. Zhou, X. He, *Sci. Adv.* **2020**, 6.
- [20] T. Mirfakhrai, J. D. W. Madden, R. H. Baughman, *Mater. Today* **2007**, 10, 30.